**Title:** Pd decorated Co-Ni nanowires as a highly efficient catalyst for direct ethanol fuel cells

**Author:** Dariusz Łukowiec, Tomasz Wasiak, Dawid Janas, Elżbieta Drzymała, Joanna Depciuch, Tomasz Tarnawski, Jerzy Kubacki, Stanisław Wacławek, Adrian Radoń

**Citation style:** Łukowiec Dariusz, Wasiak Tomasz, Janas Dawid, Drzymała Elżbieta, Depciuch Joanna, Tarnawski Tomasz, Kubacki Jerzy, Wacławek Stanisław, Radoń Adrian. (2021). Pd decorated Co-Ni nanowires as a highly efficient catalyst for direct ethanol fuel cells. „International Journal of Hydrogen Energy" (Vol. 0, iss. 0, 2021, s. 1-15), DOI: 10.1016/j.ijhydene.2021.11.177

Available online at www.sciencedirect.com

ScienceDirect

journal homepage: www.elsevier.com/locate/he

# Pd decorated Co–Ni nanowires as a highly efficient catalyst for direct ethanol fuel cells

*Dariusz Łukowiec* [a,*], *Tomasz Wasiak* [b], *Dawid Janas* [b], *Elżbieta Drzymała* [c], *Joanna Depciuch* [c], *Tomasz Tarnawski* [c], *Jerzy Kubacki* [d,e], *Stanisław Wacławek* [f], *Adrian Radoń* [a,g]

[a] *Materials Research Laboratory, Faculty of Mechanical Engineering, Silesian University of Technology, Konarskiego 18 a, 44-100, Gliwice, Poland*

[b] *Faculty of Chemistry, Silesian University of Technology, B. Krzywoustego 4, 44-100, Gliwice, Poland*

[c] *Institute of Nuclear Physics Polish Academy of Sciences, Radzikowskiego 152, 31-342, Kraków, Poland*

[d] *A. Chełkowski Institute of Physics, University of Silesia, 75 Pułku Piechoty 1A, 41-500, Chorzów, Poland*

[e] *Silesian Center for Education and Interdisciplinary Research, 75 Pułku Piechoty 1, 41-500, Chorzów, Poland*

[f] *Institute for Nanomaterials, Advanced Technologies and Innovation, Technical University of Liberec, Studentská 1402/2, 461 17 Liberec 1, Czech Republic*

[g] *Łukasiewicz Research Network - Institute of Non-Ferrous Metals, Sowińskiego 5 St., 44-100, Gliwice, Poland*

## HIGHLIGHTS

- Co–Ni with Pd NPs exhibit exceptional catalytic activity towards the EOR.
- Co–Ni in the ratio of 3:7 showed best catalytic properties.
- The balance between oxidized, disordered and crystalline phases of Co–Ni is the key.
- Synergistic effect of 1D morphology and structure of the Co–Ni with Pd NPs.
- The presence of Pd, $PdO_2$, Co–Ni and their oxides enhances catalytic activity.

## GRAPHICAL ABSTRACT

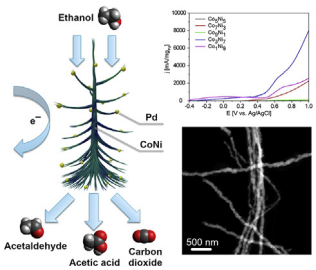


## ARTICLE INFO

*Article history:*
Received 13 August 2021
Received in revised form
5 November 2021
Accepted 22 November 2021
Available online xxx

## ABSTRACT

The storage and conversion of energy necessitates the use of appropriate electrochemical systems and chemical reaction catalysts. This work presents newly developed catalysts for electrooxidation of ethanol in an alkaline medium. Nanocatalysts composed of Co–Ni nanowires (Co–Ni NWs) decorated with Pd nanoparticles (Pd NPs) were made at varying metal ratios and their chemical composition and structure was investigated in detail. The synthesis involved a wet chemical reduction assisted by a magnetic field, which led to the generation of NWs, followed by the deposition of spherical Pd NPs on their surface. The

* *Corresponding author.*
E-mail address: Dariusz.Lukowiec@polsl.pl (D. Łukowiec).

https://doi.org/10.1016/j.ijhydene.2021.11.177

*Keywords:*
Co–Ni nanowires
Pd nanoparticles
Ethanol oxidation reaction
Electrocatalyst
Direct ethanol fuel cells
Metallic oxides

best catalytic activity was obtained for the catalyst made of $Co_3$–$Ni_7$ decorated with Pd NPs, which exhibited EOR of 8003 mA/$mg_{Pd}$ for only 0.86 wt% of Pd loading. The results can be explained by the synergistic effect between the morphology of the bimetallic support and the favorable interaction of oxophilic Co, Ni with catalytic Pd.



## Introduction

The electricity demand constantly increases along with the technological development of the countries. At the same time, progressive climate change in our environment urges the society to replace energy obtained from conventional sources (fossil fuels) with those of renewable origins. Such sustainable energy may come from the sun, wind, hydropower, tidal forces, etc. [1–4]. The generated green electricity can then be directly transmitted to customers to fulfill the current needs. However, due to the intermittent nature of these energy sources and the fact that the electricity generation time does not fully coincide with the demand, there is a need to preserve it for later use. Alternatively, the energy can be extracted from chemical transformations of replenishable chemical compounds to generate electricity inside of fuel cells. Therefore, the process of energy storage and conversion requires appropriate electrochemical systems and catalysts to carry it out effectively. Due to the tremendous social and economic importance of the energy deficit problem, scientists focus on the development of new catalysts which can promote this process [5].

Direct alcohol fuel cells (DAFCs) are certainly among the most efficient fuel cells operating at ambient temperature [6–8]. The principle of their work is based on the direct conversion of chemical energy accumulated in alcohols into electric energy, which may constitute an alternative power source for vehicles, portable electronics, or other devices [9–12]. Furthermore, it is easy to store, handle, and transport liquid fuels (methanol, ethanol, 1-propanol, ethylene glycol), which can feed for fuel cells. These chemicals exhibit high availability and low costs, as compared to gaseous fuels [13–17]. Some of them can even be generated by sustainable routes. Ethanol stands out among these substrates, as it is characterized by high energy density (6.8 kWh/L), low toxicity and high bioavailability. For instance, it can be obtained by fermentation of biomass that contains sugar [11,13,18–20]. Therefore, it is not surprising that the scientific community takes such a great interest in the topic of direct ethanol fuel cells (DEFCs) [12,14,21–23]. Commonly used ethanol oxidation catalysts operating in DEFCs include Pt-based systems. However, despite its advantages such as high catalytic activity at low temperature, platinum suffers severe limitations [14,24,25]. The most important of them include high cost, low availability, and, above all, time-decreasing kinetics of ethanol oxidation reaction caused by poisoning of the catalyst with intermediate products (CHx and CO) [12,14,26–30]. Simultaneously, the use of ethanol as a fuel is associated with an additional difficulty. It is energetically challenging to break down the C–C bond to enable its conversion into $CO_2$. Consequently, the reaction efficiency does not match expectations even when Pt is engaged [31,32]. Therefore, it is essential to devise catalytic systems for ethanol oxidation to $CO_2$, which could address this problem [33].

The complete oxidation of an ethanol molecule to $CO_2$ becomes possible upon optimizing several factors such as substrate concentration, reaction temperature, type of environment (acid or alkaline), and the morphology/chemical composition of the catalyst [26,34–36]. Earlier studies conducted on the type of using medium have shown that the kinetics of both ethanol oxidation (EOR) and oxygen reduction (ORR) reactions occur faster and more efficiently in alkaline media [37–40]. Using alkaline conditions makes it possible to reduce the amount of used catalysts or enables one to employ non-Pt catalysts (nickel, silver) in the reactions [24,41], which reduces the overall cost of the process. To further alleviate the cost burden, numerous groups of researchers [29,42,43] have focused on finding a worthy replacement for Pt in alkaline direct ethanol fuel cells (ADEFCs). Higher availability which leads to lower costs, higher stability and poisoning tolerance, and above all, higher electrocatalytic activity towards EOR in alkaline medium, is provided by palladium [12,29,44–46].

Furthermore, alloying of palladium with other metals (Cu, Ag, Au, Sn, Co or Ni) [14,45,47] or metal oxides ($CeO_2$, NiO, $Co_3O_4$) [13] can improve its stability and catalytic activity in alkaline environments due to a bifunctional mechanism. In addition, it can also facilitate the formation of $OH_{ads}$ species on its surface, which minimizes the effect of catalyst poisoning by CO [13,14,45,47,48]. With this in mind, the ongoing work focuses on the preparation of efficient and stable catalysts for the oxidation of alcohols that should be less dependent on the noble metals. For instance, a proper selection of the catalyst substrate may be beneficial. Its composition and morphology were found to significantly impact on the catalytic performance [49–52]. Nowadays, the commonly used supports for metallic catalysts (Pt, Pd, Ru) include nanostructured carbon materials such as graphene, graphene oxide or carbon nanotubes. Their advantages include high specific surface area and electrical conductivity [26,53–57]. However, they cannot catalyze ethanol oxidation themselves. Their second major limitation is related to

corrosion and, consequently, to the detachment of catalyst particles from the support. Therefore, they have been looking for alternatives in the form of other supports. This work also seeks to make a contribution in this field.

It was recently found that metallic supports are capable of changing this situation. For instance, a system consisting of a Ni sponge decorated with Pd exhibited high stability and superior catalytic activity [58]. Furthermore, Pd-based catalyst systems with different morphology (PdNi nanosphere, PdNi film and PdCu aerogel) also demonstrated appreciable performance in this area [59,60]. Recently, nanowires (NWs) have attracted particular interest among researchers for this application. In the literature, there are many examples of nanocomposites containing metallic NWs, which were then evaluated for the electro-oxidation performance of methanol or ethanol such as Pt NPs/NbC NWs [61], Pd NPs/rGO-C@TiC NWs [62], Pd NWs/C [63], and Pt–Mo–Ni NWs [64]. Unfortunately, most of the presented supports are expensive and complicated in production. Therefore, this challenge asks for more suitable NW materials to be used substrates for the catalysts. Ideally, NWs should also actively participate in the catalytic reaction to increase its efficiency.

It seems that non-precious metals can play such a role. For example, nickel nanowires (Ni NWs) have already been successfully tested in urea oxidation reactions [65] and others [66]. Moreover, it was observed that the deposition of selected co-catalysts in the form of noble metal nanoparticles on the surface of Ni NWs significantly increases their catalytic activity. For example, it was shown that Ni NWs decorated with 10 wt % Pd nanoparticles have notable catalytic performance (1479.79 mA/$mg_{Pd}$ EOR) [67]. In another study [68], an efficient electrocatalyst constructed from Ni NWs with flower-like Pd NPs operating in alkaline medium showed excellent activity (765 mA/$mg_{Pd}$ EOR) also based on deposited on them. Cobalt is another example of a non-precious metal used with Pd in the nanostructure form (Co–Pd NWs), for which the obtained catalyst exhibited several times better stability and catalytic activity compared to commercial Pd/C [69]. In light of the foregoing, inexpensive and stable non-precious metals Co and Ni are highly promising materials to support precious metal catalysts. The use of metallic support in the form of nanowires (1D) can promote faster diffusion through liquid alcohol, reduce surface energy, and improve electron transport [67,68]. Importantly, Ni and Co have oxophilic nature, which increases the tolerance to the poisoning of the noble metal by CO, and thus increases its catalytic efficiency and longevity [67,70]. Therefore, an interesting issue seems to be the synthesis of bimetallic NW supports, containing both Ni and Co, to further increase the catalytic properties of the catalyst, such as Pd, deposited onto them.

The study presents two series of nanocomposites made of Co–Ni bimetallic nanowires (CoNi NWs) at varying Co:Ni ratios (5:5, 3:7, 1:9, 7:3, 9:1) with Pd NPs deposited on their surface at two precursor concentrations of 0.5 mM and 0.75 mM. The material synthesized by our group is a new generation catalyst. When developing the catalyst, it has taken into account its crystallographic structure, chemical composition and shape. These three parameters appear to be key in the context of designing next-generation catalysts. In addition, the new approach of replacing the carbon support with bimetal nanowires has improved the catalytic performance by actively participating the support in the catalysis reaction and avoiding its corrosion. The one of the goal was to develop an efficient EOR catalyst while minimizing the loading of the Pd nanoparticles. Furthermore, the metal ratios of the Co:Ni support were varied to thoroughly analyze how this affects the catalytic performance of the system. The synthesis of CoNi NWs was based on wet chemical reduction assisted with the magnetic field, on which spherical Pd NPs were then deposited. The relationship between the physicochemical properties of the obtained materials and their electrocatalytic activity in alkaline medium was studied in detail. The choice of Co and Ni as support materials was related to their oxophilic nature, which should enhance the catalytic activity of the Pd catalyst [70,71]. To the best of the authors' knowledge, it is the first demonstration of the use of bimetallic CoNi NWs as support in EOR reactions. The obtained results highlight that the 1D morphology of the support and bifunctional mechanism between CoNi and Pd improve the catalytic activity.

In this manuscript, nanocatalysts made of Co–Ni NWs with Pd NPs deposited on their surface were synthesized. Subsequently, these materials were characterized by XRD, STEM, HRTEM and XPS techniques. Finally, the catalytic properties of the obtained materials were evaluated by three-electrode electrochemical system.

## Experimental

### *Materials*

Nickel (II) chloride hexahydrate (Acros Organics, Geel, Belgium, 97%), cobalt (II) chloride hexahydrate (Chempur, Piekary Slaskie, Poland, pure p.a.), chloroplatinic acid hexahydrate (Sigma Aldrich, ACS reagent, >37.5% Pt basis), hydrazine monohydrate (Alfa Aesar, 98%), ethylene glycol (EG; Chempur, Piekary Slaskie, Poland, pure p.a.), sodium hydroxide (Chempur, Piekary Slaskie, Poland, pure p.a.), polyvinylpyrrolidone (PVP; Alfa Aesar M.W. 1 300 000, pure p.a.) were all procured from the above-mentioned vendors and used without any further purification.

### *Synthesis of cobalt–nickel nanowires (CoNi NWs)*

The modified synthesis procedure was based on the work of Zhang et al. [72]. 70 mL of 0.1 M NaOH solution in ethylene glycol (EG) was mixed with 5 mL of 64% hydrazine hydrate aqueous solution in a beaker. Then, the mixture was heated up to 90 °C, and 22 mL of precursor solution (various volume ratios of $CoCl_2$ and $NiCl_2$ salts - 1:9, 3:7, 5:5, 7:3, 9:1 dissolved in EG, and 2 mL of 0.01 M $H_2PtCl_6$ in water) was slowly dripped over 5 min. The formation of NWs was conducted for 10 min in the presence of a magnetic field established by a neodymium magnet. The magnet was enclosed by a second beaker positioned in the centre of the first beaker, where the reaction occurred (Fig. 1). After the reaction, the black magnetically active powder was separated and washed several times with distilled water and acetone to remove the by-products. Once the material was dry, it was stored in a desiccator. The samples were labelled according to the ratio of the metal precursor

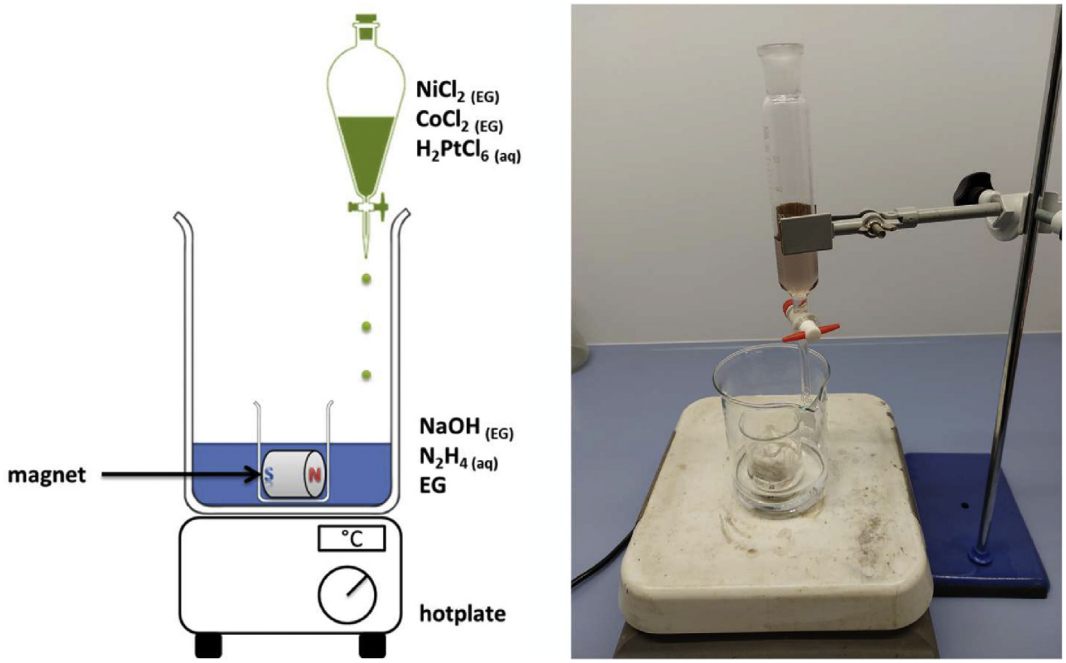


**Fig. 1 – Laboratory workstation used for the synthesis of Co–Ni NWs.**

used, i.e., a ratio of 1:9 corresponds to a $Co_1$–$Ni_9$ sample, and so on.

### *Synthesis of CoNi NWs_Pd NPs nanocomposites*

100 mL of $K_2PdCl_4$ water solution in specified concentration was poured into a three-necked round-bottom flask. 100 mg of PVP and 120 mg CoNi NWs were added to the solution, and the flask was purged with inert gas. Then the flask was inserted into the ultrasonic water bath (Bandelin Sonorex RK 102H, 320 W, 35 kHz). The mixture was heated up to 60 °C and sonicated for 1 h under an inert atmosphere. After the reaction, Pd/CoNi nanocomposites were separated and washed with copious amounts of distilled water and acetone. Once the material was dry, it was stored in a desiccator.

### *Materials characterization*

The structure and morphology of synthesized nanocomposites were determined based on transmission electron microscope (TEM) and scanning – transmission electron microscope (STEM) images, electron diffraction patterns (ED) and Energy-dispersive X-ray spectra (EDS), which were collected using Transmission Electron Microscope S/TEM TITAN 80–300. The phase composition and purity of the materials were determined by using X-ray diffractometer Rigaku MiniFlex 600 with a copper tube Cu Ka (k = 0.15406 nm). The data were analyzed by the Rietveld refinement using the Rigaku PDXL software suite. The chemical composition and electronic structure of the samples were examined by X-ray photoelectron spectroscopy (XPS) using a monochromatic X-ray source (Al $K_\alpha$, $h\nu = 1486.6$ eV; PHI5700 Physical Electronics spectrometer). The measurements were performed directly from the oxidized surface of obtained samples and after etching by $Ar^+$ ion beam with energy 2 kV for 20 min. The survey spectra and core lines of $Ni2p_{3/2}$, $Co2p_{1/2}$, Ni3s, Co3s, Pd3d, O1s, C1s, and valence band were recorded. The $Co2p_{1/2}$ line was chosen for analysis because the $Co2p_{3/2}$ line was overlapped with the NiLMM Auger transition. Atomic concentration calculations and fitting process were performed using MULTIPAK software from Physical Electronics (ver. 9.9.0.8). Metal concentrations in the samples were determined by ICP/OES (PerkinElmer, Optima 2100 DV). The samples were diluted in order to reach the appropriate concentration range. The calibrations were made with standards purchased from Sigma-Aldrich company.

### *Electrochemical measurements*

All electrochemical measurements were conducted on a BIOLOGIC SP-200 potentiostat. A conventional three-electrode electrochemical system was used with a glassy carbon electrode as the working electrode, a platinum wire as the counter electrode, and a silver chloride electrode (Ag/AgCl) as the reference electrode, respectively. Uniform catalyst inks were prepared by ultrasonically mixing 2 mg of catalysts powder (in the form of CoNi NWs with different Co:Ni mass ratios decorated with Pd NPs) with the solution containing isopropyl alcohol and 5 wt % Nafion solution for 30 s. Next, 10 μl of as-prepared ink suspension was deposited onto a polished glassy carbon electrode (GCE) to obtain the working electrode with a homogenous thin catalyst layer after the solvent dried naturally in the air. All the electrochemical experiments were conducted at ambient temperature. Prior to electrochemical measurements, the electrolytes containing fresh-prepared 1 M NaOH with 0.5 M or without ethanol, were deoxygenated by bubbling with Ar for 30 min. Then, CV measurements in ethanol-containing solution were carried out to determine

**Table 1 – Deposition of Pd NPs on CoNi NWs by varying concentrations of Pd ions during reactions.**

| Sample | NWs composition | $C(K_2PdCl_4)$ [mM] | Pd content [% wt] |
|---|---|---|---|
| 1 | $Co_1$–$Ni_9$ | 0.5 | 0.88 |
| 2 | $Co_3$–$Ni_7$ | 0.5 | 0.81 |
| 3 | $Co_5$–$Ni_5$ | 0.5 | 0.83 |
| 4 | $Co_7$–$Ni_3$ | 0.5 | 1.54 |
| 5 | $Co_9$–$Ni_1$ | 0.5 | 0.85 |
| 6 | $Co_1$–$Ni_9$ | 0.75 | 1.92 |
| 7 | $Co_3$–$Ni_7$ | 0.75 | 0.86 |
| 8 | $Co_5$–$Ni_5$ | 0.75 | 3.35 |
| 9 | $Co_7$–$Ni_3$ | 0.75 | 2.96 |
| 10 | $Co_9$–$Ni_1$ | 0.75 | 1.41 |

these catalysts' ethanol oxidation reaction (EOR) activity. The electrochemical data were normalized by the Pd mass of each catalyst (in mg) obtained by inductively coupled plasma (ICP) measurements.

## Results and discussions

### *Structure and morphology analysis*

The synthesis of Pd NPs/CoNi NWs revealed that even if the same concentration of Pd precursor is used for the deposition, the resulting concentration of Pd is different depending on the employed conditions (Table 1). This shows that the Pd loading on the surface of CoNi NWs is structure- or morphology-dependent. To determine the role of these factors on the possibility of deposition of Pd NPs, the structural analysis was performed using transmission electron microscopy, X-ray diffraction method, and X-ray photoelectron spectroscopy. First of all, XRD patterns were measured and compared for two series of CoNi NWs with different Co:Ni ratios and Pd precursor concentrations (Fig. 2a and b). The obtained XRD patterns confirm that the structure of CoNi NWs is strongly Co:Ni ratio-dependent. Additionally, the Rietveld refinement method was used to determine the absence of the other phases and the presence and cell parameters of the identified ones. The analysis results were presented in Table 2 together with the fitting parameters: weighted profile residual ($R_{wp}$), profile residual ($R_p$), and goodness of fit ($\chi^2$). As one can see, the fitting parameters confirm the presence of two phases in all samples, generally, Ni(Co) and $Co_{0.75}Ni_{25}$ ones. When the concentration of Ni precursor is much higher than $Co^{2+}$ precursor 9:1 and 7:3 ($Co_1$–$Ni_9$ - orange curve and $Co_3$–$Ni_7$ - green curve), the dominant phase is the cubic Ni(Co) (space group: Fm-3m). With increasing content of $Co^{2+}$ precursor, the crystallization of this phase becomes difficult, and thus the highly disordered hexagonal $Co_{0.75}Ni_{0.25}$ phase (space group: P63/mmc) crystallizes ($Co_9$–$Ni_1$ - black curve, $Co_7$–$Ni_3$ - red curve). Interestingly, when the concentration of the palladium precursor is equal to 0.75 mM, it is possible to identify the characteristic for crystalline CoPd (space group: Fm-3m) (111) peak. However, only for the sample with the highest Ni concentration (Fig. 2b - $Co_1$–$Ni_9$ - orange curve). Probably, it is related to the growth of Pd NPs on the surface of Ni(Co) in well-ordered

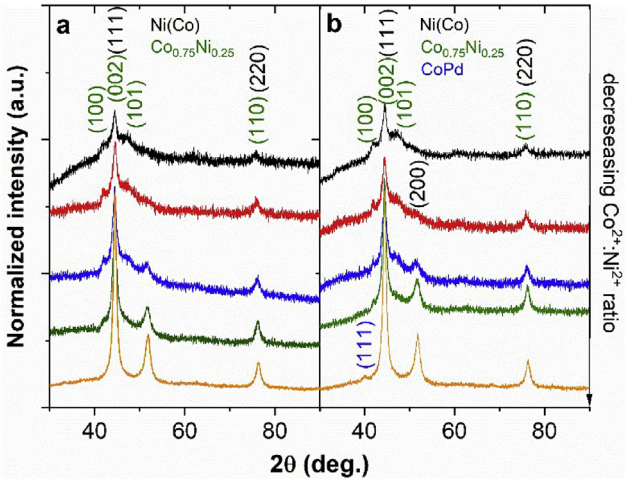


**Fig. 2 – XRD patterns of CoNi NWs synthesized using different Co:Ni ratios with marked peaks corresponding to the Ni(Co), $Co_{0.75}Ni_{25}$ phases and CoPd. Samples synthesized using 0.5 mM (a) and 0.75 mM (b) of $K_2PdCl_4$. ($Co_9$–$Ni_1$ - black curve, $Co_7$–$Ni_3$ - red curve, $Co_5$–$Ni_5$ - blue curve, $Co_3$–$Ni_7$ - green curve, $Co_1$–$Ni_9$ - orange curve). (For interpretation of the references to colour in this figure legend, the reader is referred to the Web version of this article.)**

crystallites (both phases crystallize in similar unit cells). In contrast, the same situation cannot occur when Pd growth occurs on the NWs composed predominantly from hexagonal $Co_{0.75}Ni_{0.25}$ phase.

To determine the co-existence of both identified phases and their role in the formation of Pd NPs, TEM and EDX analyses were also performed. Firstly, in Fig. 3a–f, the morphology of three samples (NWs with deposited Pd NPs) with different Co:Ni ratios (9:1, 5:5, and 3:7) was compared. It is evident that all analyzed samples form NWs, however, their surface morphology is different. The needle-like surface shape can be observed for samples containing high nickel concentration (composed of almost pure Ni(Co) cubic phase). On the other hand, for samples with high Co concentration, the wires are composed of spherical-shaped particles, which are probably related to the existence of highly disordered $Co_{0.75}Ni_{0.25}$ phase. Moreover, the surface of these wires is surrounded by a plate-like structure (Fig. 3b). The presence of both ball-like and needle-like particles is related to the metallic Ni–Co, whereas the observed plates result from the presence of cobalt and nickel oxides, which was confirmed through EDX spectra analysis (Fig. 3g and h). Interestingly, as shown in Fig. 3g and h, the palladium presence was observed at the edges of the cobalt and nickel oxide layers (area 1 on Fig. 3g). According to that, while the concentration of Ni and Co plays a crucial role in the formation of wires with two different surface morphologies, the existence or absence of an oxidized surface should reflect in the formation of Pd NPs.

The concentration of this oxidized surface is also Co:Ni ratio-dependent. When NWs are composed of ultra-fine crystallites of hexagonal $Co_{0.75}Ni_{0.25}$ phase, the oxidized layers form a plate-like structure. However, when the

**Table 2 – Identified, on XRD patterns, phases with the cell parameters and fitting parameters ($R_{wp}$, $R_p$, and $\chi^2$).**

| Sample | Identified phases | Space group | Cell parameters | $R_{wp}$ (%) | $R_p$ (%) | $\chi^2$ |
|---|---|---|---|---|---|---|
| 0.5 mM of $K_2PdCl_4$ | | | | | | |
| $Co_9$–$Ni_1$ | Ni(Co) | Fm-3m | a = b = c = 3.528 Å; α = β = γ = 90° | 1.46 | 1.15 | 1.04 |
| | $Co_{0.75}Ni_{25}$ | P63/mmc | a = b = 2.721 Å; c = 4.078 Å; α = β = 90°; γ = 120° | | | |
| $Co_7$–$Ni_3$ | Ni(Co) | Fm-3m | a = b = c = 3.5404 Å; α = β = γ = 90° | 1.64 | 1.29 | 1.34 |
| | $Co_{0.75}Ni_{25}$ | P63/mmc | a = b = 2.452 Å; c = 4.182 Å; α = β = 90°; γ = 120° | | | |
| $Co_5$–$Ni_5$ | Ni(Co) | Fm-3m | a = b = c = 3.5404 Å; α = β = γ = 90° | 1.72 | 1.32 | 1.43 |
| | $Co_{0.75}Ni_{25}$ | P63/mmc | a = b = 2.516 Å; c = 4.407 Å; α = β = 90°; γ = 120° | | | |
| $Co_3$–$Ni_7$ | Ni(Co) | Fm-3m | a = b = c = 3.5389 Å; α = β = γ = 90° | 1.81 | 1.33 | 1.55 |
| | $Co_{0.75}Ni_{25}$ | P63/mmc | a = b = 2.602 Å; c = 3.814 Å; α = β = 90°; γ = 120° | | | |
| $Co_1$–$Ni_9$ | Ni(Co) | Fm-3m | a = b = c = 3.5316 Å; α = β = γ = 90° | 2.19 | 1.53 | 1.96 |
| | $Co_{0.75}Ni_{25}$ | P63/mmc | a = b = 2.355 Å; c = 3.830 Å; α = β = 90°; γ = 120° | | | |
| 0.75 mM of $K_2PdCl_4$ | | | | | | |
| $Co_9$–$Ni_1$ | Ni(Co) | Fm-3m | a = b = c = 3.537 Å; α = β = γ = 90° | 1.65 | 1.30 | 1.26 |
| | $Co_{0.75}Ni_{25}$ | P63/mmc | a = b = 2.548 Å; c = 4.305 Å; α = β = 90°; γ = 120° | | | |
| $Co_7$–$Ni_3$ | Ni(Co) | Fm-3m | a = b = c = 3.5460 Å; α = β = γ = 90° | 1.47 | 1.16 | 1.01 |
| | $Co_{0.75}Ni_{25}$ | P63/mmc | a = b = 2.539 Å; c = 4.095 Å; α = β = 90°; γ = 120° | | | |
| $Co_5$–$Ni_5$ | Ni(Co) | Fm-3m | a = b = c = 3.53 Å; α = β = γ = 90° | 1.78 | 1.37 | 1.49 |
| | $Co_{0.75}Ni_{25}$ | P63/mmc | a = b = 2.564 Å; c = 4.114 Å; α = β = 90°; γ = 120° | | | |
| $Co_3$–$Ni_7$ | Ni(Co) | Fm-3m | a = b = c = 3.54 Å; α = β = γ = 90° | 2.11 | 1.63 | 2.00 |
| | $Co_{0.75}Ni_{25}$ | P63/mmc | a = b = 2.526 Å; c = 4.329 Å; α = β = 90°; γ = 120° | | | |
| $Co_1$–$Ni_9$ | Ni(Co) | Fm-3m | a = b = c = 3.5276 Å; α = β = γ = 90° | 2.50 | 1.74 | 2.72 |
| | CoPd | Fm-3m | a = b = c = 3.907 Å; α = β = γ = 90° | | | |

concentration of this phase decrease, only the thin oxidized layer can be observed. To determine the role of oxidized surface on the palladium nanoparticles nucleation and growth, HRTEM images were investigated for different samples. The presence of two areas, in which Pd nanoparticles occur was confirmed for all analyzed samples and presented in Fig. 4. The performed analysis of HRTEM image of CoNi NWs with Co:Ni ratio equal to 9:1 confirmed the existence of two observed on STEM images areas related to the highly disordered core $Co_{0.75}Ni_{0.25}$ phase (green-marked area in Fig. 4a and corresponding Fig. 4b) and to the presence of oxidized plate-like surface of $PdO_2$ nanoparticles (blue marked area in Fig. 4a and corresponding Fig. 4c). Whereas the core is associated with the metallic phase, the palladium was observed especially in the form of $PdO_2$ on an oxidized surface. While $PdO_2$ crystallizes especially on the oxidized surface, some palladium NPs and atomic clusters can also be observed on the highly crystalline Ni(Co) phase (Fig. 4d–f). Furthermore, the same analysis confirms the possibility of the crystallization of metallic Pd ultra-fine particles in the oxidized surface of CoNi NWs with the Co:Ni ratio equal to 5:5 (Fig. 4g and h). To summarize, the coexistence of the Pd and $PdO_2$ NPs is related to the $Pd^{2+}$ ions nucleation and growth on both oxidized and metallic phases. However, the oxidized form crystallizes only on the oxidized NWs surface.

To confirm the coexistence of pure Pd and $PdO_2$ NPs, XPS spectra were collected for Pd/CoNi NWs with Co:Ni ratio equal to 3:7. The analysis was performed for two different Pd loadings to determine the role of Pd precursor concentration on the formation of $Pd^0$ and $Pd^{4+}$ states. For this purpose, the XPS spectra were collected and analyzed for NWs in an as-synthesized state and also after removing the oxidized surface using $Ar^+$ ion etching. The survey spectra (Fig. A.1) confirm the existence of Ni, Co, and Pd in both oxidized surface and metallic core. While the concentration of Co and Ni is similar in the surface and core (Table A1) the palladium atomic concentration is much higher on the surface than in the metallic core. The performed above analysis of TEM images assumed that all nanowires have an oxidized surface. The collection of the Ni2p photoemission spectra obtained for all investigated samples are depicted in Fig. 5a and b. All presented shapes of the $2p_{3/2}$ levels are complex because of three components at binding energies of 856.6 eV, 854.4 eV and 852.8 eV, which corresponded to the presence of $Ni_2O_3$ and NiO oxides on the oxidized surface and Ni atoms in the core of CoNi NWs, respectively [24,67,73,74]. The intensities or lack of particular components are different for all samples indicates their various contents in outer layers. The additional component at binding energies above 857 eV corresponded to the satellite structure of the main $2p_{3/2}$ line. The shapes of the $Co2p_{1/2}$ spectra presented in Fig. 5d and e consists of two components. The first of them at 797.6 eV of binding energy corresponded to $Co_3O_4$ oxides layer, while the second represented satellite structure. In order to check of the chemical composition of the core of investigated samples the ion treatment was applied by using $Ar^+$ ion gun. The obtained results were presented in Fig. 5c, f and i. In the case of nickel, the shape of $2p_{3/2}$ photoemission line indicates a metallic form of nickel in the core of CoNi alloy (Fig. 5c), while in the case of $Co2p_{1/2}$, except for pure cobalt, a small contribution of oxides form still existed (Fig. 5f). This may be due to the significant surface roughness of the core, which does not allow complete removal of the oxidized outer layer of the core. Interestingly, also the analysis of Pd $3d_{3/2}$ and Pd $3d_{5/2}$ high-resolution XPS spectra confirm the possibility of crystallization of both Pd and $PdO_2$ nanoparticles. Moreover, as can be seen in Fig. 5g and h, the signal from $PdO_2$ is strongly related to the concentration of the used precursor. While the concentration of Pd precursor was equal to 0.5 mM, the existence of a strong peak from the $PdO_2$ can be visible. For 0.75 mM the

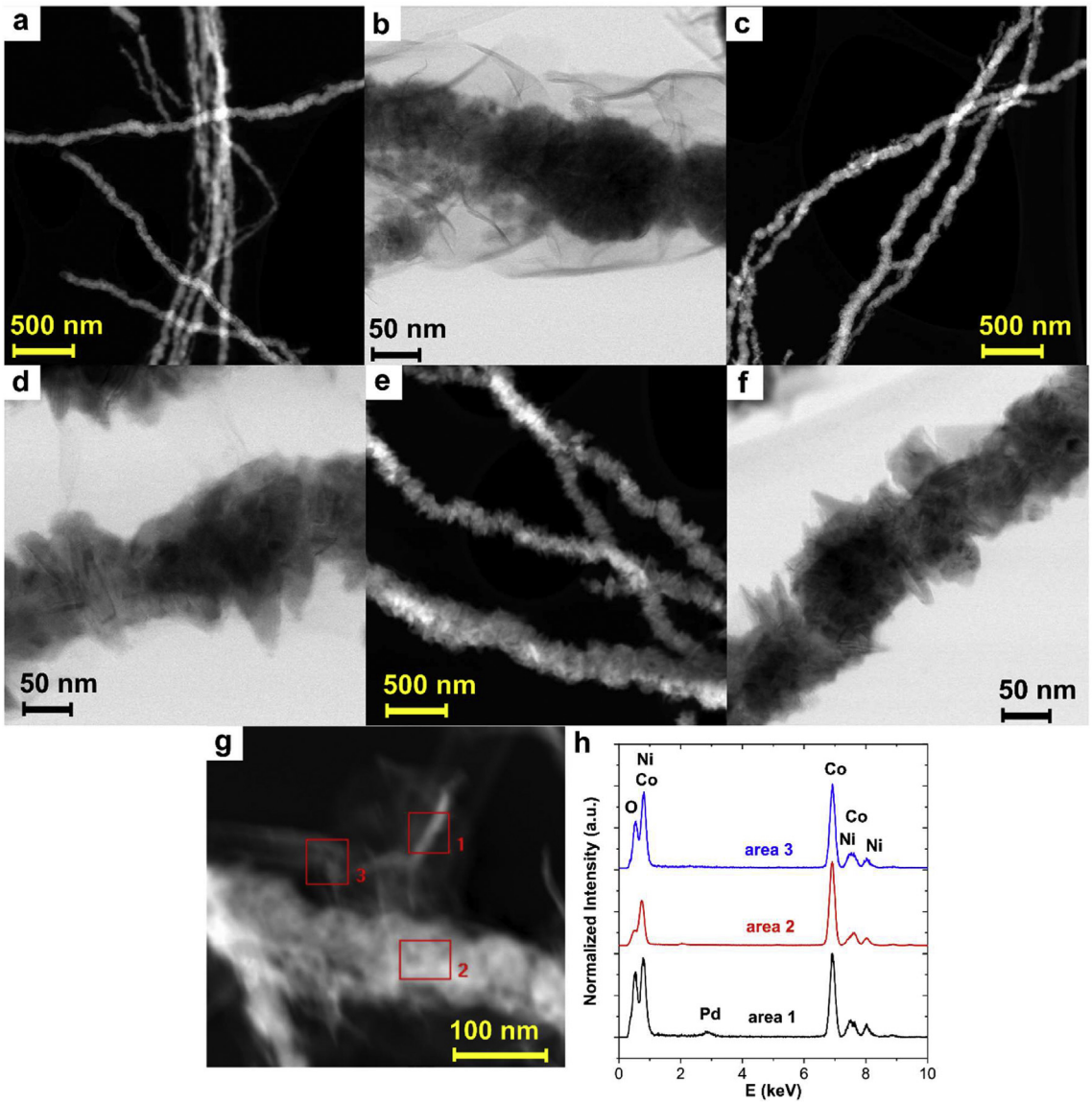


**Fig. 3 – STEM HAADF (a, c, e) and BF-DF (b, d, f) images of CoNi NWs synthesized using different Co:Ni precursor ratios: 9:1 (a, b), 5:5 (c, d) and 3:7 (e, f); (g) HAADF STEM image of CoNi NW synthesized using Co:Ni precursor ratio equal to 9:1 with marked areas and corresponding to them EDX spectra (h) confirming existence of Co and Ni oxides and Pd nanoparticles deposited on this oxidized surface.**

intensity of peak related to the $PdO_2$ is much smaller. With the increasing concentration of $Pd^{2+}$ ions, it is more favorable to crystallize the metallic Pd NPs. For lower concentrations, firstly, $PdO_2$ crystallizes, especially on the oxidized surface of NWs (Fig. 5g–i). While the formation of the $PdO_2$ is strongly related to the interaction with $Ni_2O_3$, NiO, and $Co_3O_4$ oxides, the formation of metallic Pd is related to their crystallization of the surface of the CoNi core, which manifests itself in the formation of ultra-fine NPs and atomic clusters of Pd on the surface of highly crystalline Ni. Probably the formation of metallic Pd nanoparticles on the oxides is limited. A comparison of the binding energy of particular components of the photoemission lines of Ni 2p3/2, Co $2p_{1/2}$ and Pd 3d5/2 for samples $Co_3$–$Ni_7$ with deposited Pd NPs in concentration of 0.5 and 0.75 mM of $K_2PdCl_4$ was presented in Table 3.

### *Electrochemical analysis*

The cyclic voltammetry measurements were used to determine the electrochemical behavior and verify the catalytic properties of the catalysts synthesized by using two different concentrations of Pd precursor, 0.5 and 0.75 mM. Two series of electrocatalyst samples were prepared by depositing Pd NPs on Co–Ni NWs with different Co:Ni ratios. Fig. 6 shows the cyclic voltammograms (CVs) of Co:Ni NWs decorated by Pd NPs, obtained in a standard three-electrode electrochemical cell at a scan rate of 20 $mVs^{-1}$ in 1 M NaOH without ethanol. CV results for catalysts synthesized by using 0.5 mM palladium precursor were marked by a dashed line and for 0.75 mM by a solid line, $Co_7$–$Ni_3$ – red, $Co_3$–$Ni_7$ – blue, and $Co_1$–$Ni_9$ – magenta curve, respectively. The results for $Co_5$–$Ni_5$ and

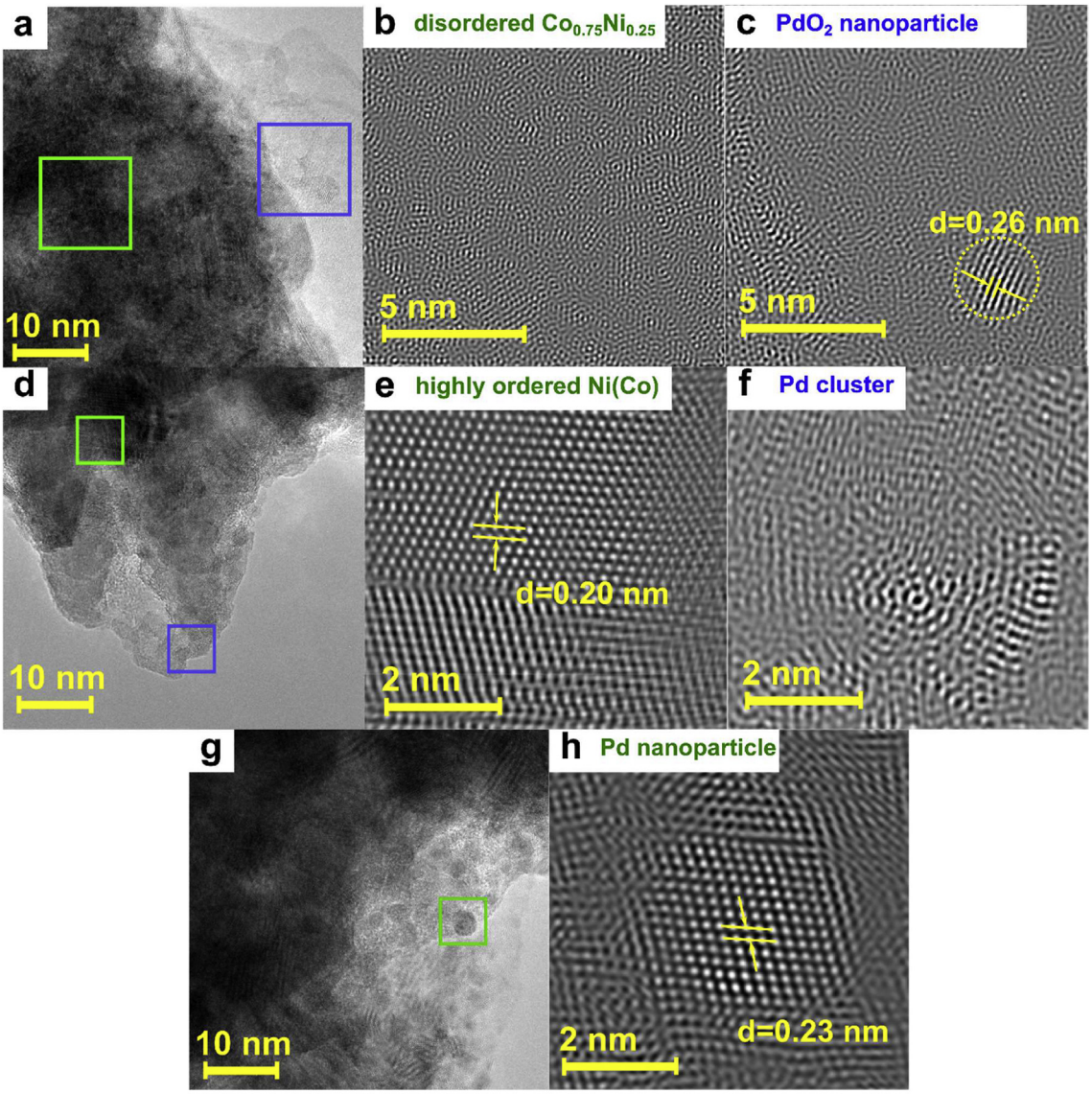


**Fig. 4 – HRTEM micrographs of CoNi NWs synthesized using Co:Ni precursors ratio: 9:1 (a-c), 3:7 (d-f) and 5:5 (g and h); (b) enlarged green marked area on (a) confirming existence of highly disordered $Co_{0.75}Ni_{0.25}$ hexagonal structure; (c) enlarged blue-marked area on (a) with identified interplanar distance characteristic for $PdO_2$ (101) planes; (e) enlarged green-marked area on (d) with identified interplanar distance characteristic for Ni (111) planes; (f) enlarged marked blue area on (d) confirming the existence of Pd atomic clusters at the edges of highly crystalline Ni phase; (h) enlarged green marked area on (g) with identified interplanar distance characteristic for Pd (111) planes. (For interpretation of the references to colour in this figure legend, the reader is referred to the Web version of this article.)**

$Co_9$–$Ni_1$ nanowires for both Pd precursor concentrations are presented in the supplementary information (Fig. A.2). Fig. A.2 shows an overview of CV curves for all five catalysts obtained by using 0.5 (a) and 0.75 (b) mM Pd precursor for easier comparison. The profiles presented in Fig. 6 correspond to the fifth cycle of the respective catalysts. According to the literature reports, the peaks above 0.3 V were assigned to the oxidation of Pd to palladium oxide, and the reduction of the oxides thus formed [78]. It should be noted that the palladium percentage is only about 1%. In comparison to other works, where the mass fraction of Pd is 10% [67] or even 22% [73], may be noticeable differences in the intensity of these peaks.

Because nano-structural architecture plays a crucial role in the catalytic activity, decoration method in synthesis of electrocatalysts and the synthesis of nanocatalysts with sophisticated shapes, became very popular and allow to obtain very high electrocatalytic activity. Therefore, inspired by these findings, we tested our catalysts in 1.0 M NaOH + 0.5 M $C_2H_5$-OH solution in order to investigate their catalytic ability towards ethanol oxidation. After adding ethanol into the electrolyte, the solution was bubbled with inert gas (Ar) for 30 min, and the experiment was continued. Fig. 7a shows the cyclic voltammograms of ethanol oxidation under alkaline conditions (0.5 M $C_2H_5OH$ and 1 M NaOH) for the two series of

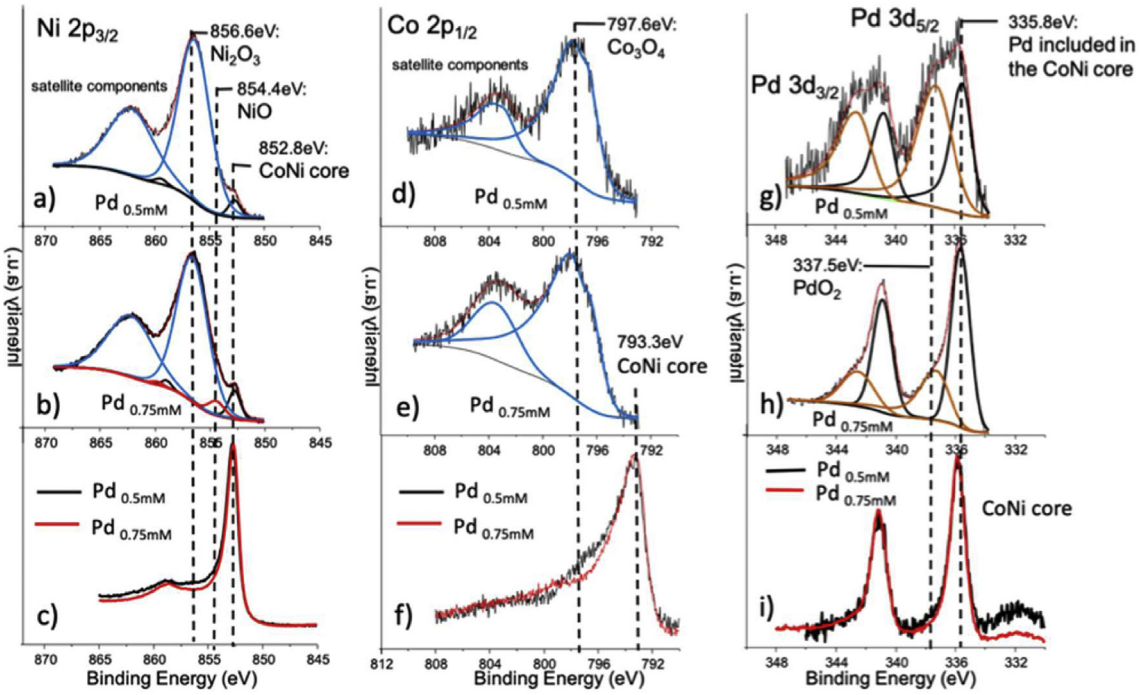


**Fig. 5 – Ni2p$_{3/2}$ (a, b and c), Co2p$_{1/2}$ (d, e and f) and Pd3d$_{5/2}$ (g, h and i) photoemission spectra recorded for CoNi NWs (Co:Ni ratio equal to 3:7) after deposition of Pd NPs using 0.5 mM of $K_2PdCl_4$ (a, d, g) and 0.75 mM of $K_2PdCl_4$ (b, e, h); the spectra on (c, f and i) were obtained after $Ar^+$ ion treatment procedure.**

**Table 3 – The binding energy of particular components of the photoemission lines of Ni 2p3/2, Co 2p$_{1/2}$ and Pd 3d5/2 for samples $Co_3$–$Ni_7$ with deposited Pd NPs in concentration of 0.5 and 0.75 mM of $K_2PdCl_4$.**

| | Sample: CoNi (3:7) 0.5 mM $K_2PdCl_4$ & 0.75 mM $K_2PdCl_4$ | | | |
|---|---|---|---|---|
| | Binding Energy (eV) | | | References |
| Photoemission line | Ni 2p$_{3/2}$ | Co 2p$_{1/2}$ | Pd 3d$_{5/2}$ | |
| Ni atoms in CoNi core | 852.8 eV | | | This work |
| NiO | 854.4 eV | | | [24,67,73,74] |
| $Ni_2O_3$ | 856.6 eV | | | |
| Co atoms in CoNi core | | 793.3 eV | | This work |
| $Co_3O_4$ | | 797.6 eV | | [72,75,76] |
| Pd atoms in CoNi core | | | 335.8 eV | This work |
| $PdO_2$ | | | 337.5 eV | [14,77] |

CoNi NWs with different Co:Ni ratios and palladium precursor concentrations. CVs were recorded at 20 mV per second in the potential range from −0.4 to 1 V vs Ag/AgCl at room temperature for all synthesized catalysts. The current was normalized to the amount of Pd obtained by ICP, thus reporting mass activities. The results for $Co_5$–$Ni_5$ and $Co_9$–$Ni_1$ nanowires for both Pd precursor concentrations, similar to the CV curves, were presented in Supplementary Information (Fig. A.3 and Fig. A.4). In the case of both sample series (for different Pd precursor concentrations), $Co_5$–$Ni_5$ and $Co_9$–$Ni_1$ NWs decorated by Pd NPs showed very similar, and at the same time, low catalytic activity (Fig. A.3 and Fig. A.4). In the case of ultrahigh Co:Ni ratio equal to 9:1, the palladium form ultra-fine $PdO_2$ only at the edges of $Co_3O_4$, NiO, and $Ni_2O_3$ plate-like oxides. According to that, this oxidized palladium cannot react in any way with a metallic nanowire core. With increasing concentration of Ni precursor, this plate-like structure disappears progressively. When Co:Ni ratio is equal to 1:9, palladium can crystallize in metallic form, crystallites are large (detectable even by XRD method). These well crystalized Pd NPs are responsible for very good catalytic activity (2500 mA/mg$_{Pd}$ for 1.92% of Pd). However, which was confirmed herein, to achieve the highest catalytic activity, it is necessary to obtain a balance between highly crystalline metallic Ni(Co) cubic phase and highly disordered $Co_{0.75}Ni_{0.25}$ phase. As it can be noticed, depending on the Co:Ni ratio, the electrocatalytic activity towards ethanol oxidation reaction is changing. The different activities of studied samples could be attributed to the changes in the structure and morphology of NWs and NPs which, as shown by the XRD and TEM results, are strongly dependent on the Co:Ni ratio. According to the Fig. A.3, the catalytic activities were increasing in the

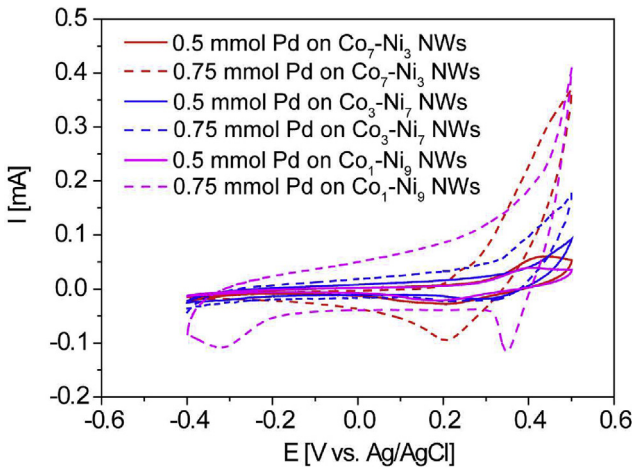


**Fig. 6 – Cyclic voltammetry curves of Co:Ni NWs decorated by Pd NPs in argon-saturated 1.0 M NaOH solution at a scan rate of 20 mV/s at room temperature. The solid lines present the results for electrocatalysts synthesized by using 0.5 mM palladium precursor, while the dashed lines by using 0.75 mM palladium precursor.**

following order: $Co_9$–$Ni_1$ < $Co_5$–$Ni_5$ < $Co_7$–$Ni_3$ < $Co_1$–$Ni_9$ < $Co_3$–$Ni_7$ for 0.5 mM concentration of Pd precursor and $Co_5$–$Ni_5$ < $Co_9$–$Ni_1$ < $Co_7$–$Ni_3$ < $Co_1$–$Ni_9$ < $Co_3$–$Ni_7$ for 0.75 mM concentration of Pd precursor (Fig. A.4), respectively. In both $K_2PdCl_4$ concentrations, the highest catalytic activity showed $Co_3$–$Ni_7$ NWs decorated by Pd NPs nanocatalysts. Mass activity for $Co_3$–$Ni_7$_Pd (0.75 mM) catalyst is more than 3 times higher compared to the other catalysts (Fig. 7). For $Co_3$–$Ni_7$_Pd (0.5 mM) and $Co_3$–$Ni_7$_Pd (0.75 mM) catalysts, the mass activities were up to 5252 mA/$mg_{Pd}$ and 8003 mA/$mg_{Pd}$, respectively. Additionally, Fig. 7c and d outlines mass activities at 0.8 and 0.9 V. As it was demonstrated in Fig. 7c and d, the $Co_7$–$Ni_3$ (red curve) and $Co_3$–$Ni_7$ NWs (blue curve) decorated by Pd NPs (0.75 mM) showed higher mass activities in comparison of sample series obtained by using 0.5 mM Pd precursors. The opposite is true only for a sample with a Co:Ni ratio of 1:9 (magenta curve).

Another important parameter describing the activity of the catalysts is the so-called onset potential, which is defined as the value of the potential at which the current rapidly rises. The lower the onset potential is, the faster the reaction starts. The EOR curves for all the catalysts in an ethanol-containing

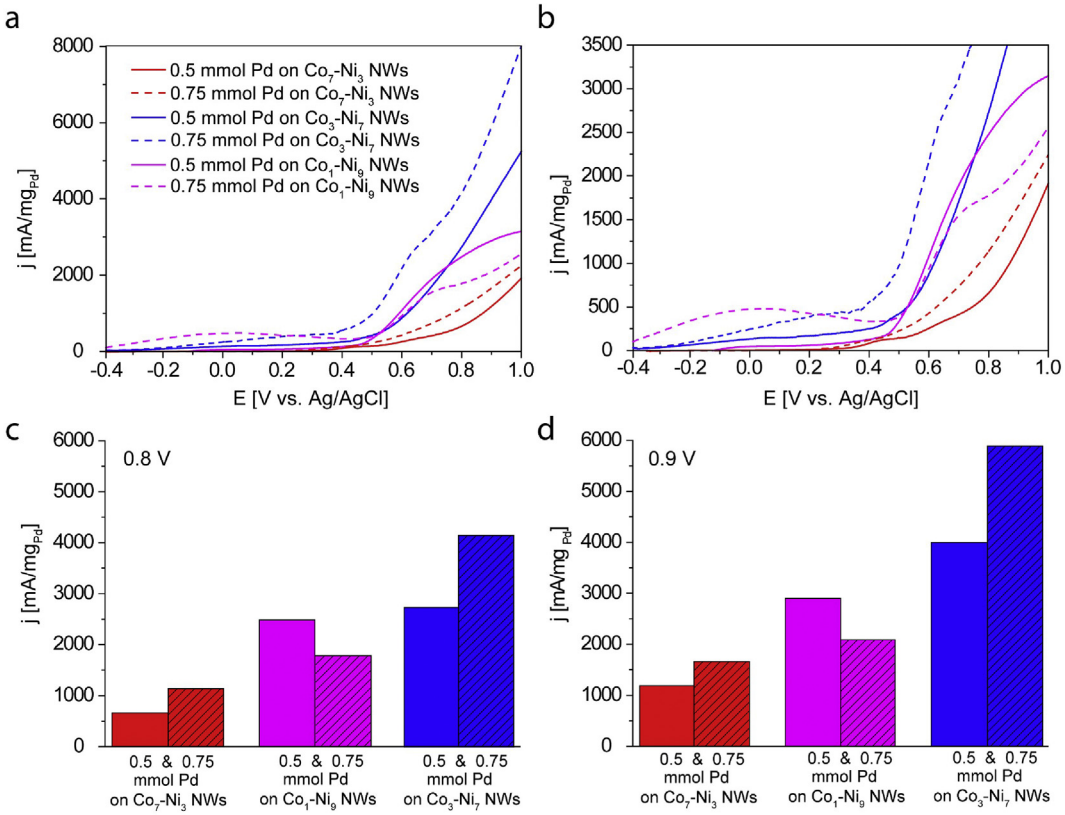


**Fig. 7 – (a) Comparison of the cyclic voltammograms (EOR curves) of electrocatalysts in the form of cobalt-nickel nanowires with different Co:Ni ratios decorated by Pd in argon-saturated 1.0 M NaOH + 0.5 M $CH_3CH_2OH$ solution at a scan rate of 20 mV/s; (b) plot showing an enlargement of the data between 0 and 3500 mA/$mg_{Pd}$; (c) EOR activities of all tested catalysts at a potential of 0.8 V and (d) 0.9 V vs. Ag/AgCl. The solid lines present the results for electrocatalysts synthesized by using 0.5 mM palladium precursor, while the dashed lines by using 0.75 mM palladium precursor. The current values were normalized by the Pd content.**

electrolyte, indicate that the onset potential of ethanol electrooxidation for the $Co_1$–$Ni_9$_Pd (0.75 mM) is the lowest. Despite that, in comparison to $Co_3$–$Ni_7$_Pd (0.75 mM) sample, the value of current densities is almost three times lower. As was deduced from the results in Fig. 7b, also for $Co_3$–$Ni_7$_Pd (0.75 mM) sample, the value of onset potential is shifted toward less positive values compared to the other four catalysts, and above 0.2 V vs Ag/AgCl has the highest value of current densities.

This superior catalytic activity of $Co_3$–$Ni_7$_Pd (0.75 mM) catalyst might be attributed to the presence of two different crystalline phases: metallic Ni(Co) cubic phase and highly disordered $Co_{0.75}Ni_{0.25}$ phase, which can be easily oxidized to the cobalt and nickel oxides. Moreover, the nanometric size of Pd nanoparticles provides a large surface area, which is desirable for electrocatalytic activity. According to the literature, all metals: palladium, nickel and cobalt are oxophilic [14,67,70,79]. Therefore, due to the oxophilic nature of Ni and Co it could spontaneously convert Ni, Co to their oxides [14,67,70], which was confirmed by XPS results (Fig. 5). These properties cause that Ni and Co have the capacity to generate $OH_{ads}$ at a lower potential and facilitate the oxidative desorption of the intermediate products, thus enhancing the catalytic activity of catalysts containing palladium, nickel, and cobalt [80,81]. Furthermore, besides the chemical composition of the tested catalysts and properties of palladium, cobalt, and nickel, definitely, the morphology of the obtained catalysts also play a crucial role in the ethanol oxidation reaction: a good dispersion of palladium nanoparticles causes larger exposed active surface area and possibly better interaction with the three metals [14].

The catalysts in the form of nanowires have already been previously reported in the literature [67,82,83]. Du et al. [82] described nanoporous $Pd_{57}Ni_{43}$ alloy NW catalysts with the mass activity of about 800 mA/$mg_{Pd}$. The authors underlined nanowires are very interesting structures as they can act as catalysts, so they do not require any support. Consequently, the detachment problems and corrosion of support that catalytic systems based on nanoparticles and support often suffered can be avoided. Similar structures based on nanowires were also synthesized by Bin et al. [83]. Nevertheless, catalyst synthesized by this group was prepared as Pd–Ni bimetallic NW networks supported on reduced graphene oxide, and the mass activity of this system was up to 604.3 mA/$mg_{Pd}$. However, in both cases, the electrocatalytic oxidation of formic acid was investigated. Kottayintavida and Gopalan synthesized [67] the Pd modified Ni NW catalyst towards methanol and ethanol electro oxidation. The authors showed that the PdNi catalyst obtained by galvanic replacement reaction achieved mass activity of about 1500 mA/$mg_{Pd}$, while for the $Co_3$–$Ni_7$_Pd (0.75 mM) catalyst synthesized in this work, the catalytic activity in EOR was more than five times higher (8003 mA/$mg_{Pd}$) (Fig. 7a). A catalyst with the same chemical composition as synthesized in this work, but a different structure, was synthesized by Zhang group [73]. However, the NiCoPd nanocatalyst was dispersed on carbon nanotubes and used as catalyst towards methanol oxidation reaction with current densities of 862 mA/$mg_{Pd}$ (9 times less than the catalyst obtained in this work).

Big advantage of catalyst synthesized in this work is lack of platinum. In case of designing catalyst often the key challenge is removal of platinum from the catalyst composition. It is related with that the platinum is susceptible to poisoning by CO-like intermediates, leading to the blockage of their active sites and the reduction of catalytic activity [84,85]. Moreover platinum is very expensive metal. Therefore a lot of studies are focused on replacement of platinum by another metals like palladium. Zhai et al. [75] also synthesized catalyst with the unique 1D nanowire structure. They system was based on Co and Pt. As they showed PtCo nanowires synthesized by them has the electrocatalytic activity in ethanol oxidation reaction of 2203 mA/$mg_{Pt}$, what is about four times lower in comparison of $Co_3$–$Ni_7$_Pd (0.75 mM) catalyst synthesized in this work.

Based on the literature, we have grounds to speculate that the synergistic interactions between Pd and CoNi nanowires promote significant enhancement of catalytic activity when the Co:Ni ratio is equal to 3:7. Thus, the enhanced performance can be attributed to the direct physical contact between CoNi NWs with Pd. The crucial role of physical contact between the respective nanoparticles was underlined in the literature frequently [26,86–88]. As was shown by Drzymala et al. [26], by choosing the appropriate metal composition and ensuring the physical contact between the nanoparticles forming the nanocatalysts, the overall catalytic activity towards the ethanol oxidation reaction and durability could be improved to a large extent. Crabb et al. [88] also noticed that catalysts are more successful when two metals are in contact with each other. Therefore, we suggest that the presence of interfaces between the NiCo NWs and Pd NPs could induce charge transfer, which enhances the catalytic performance. A comparison of our catalysts with other catalyst systems based on Pd and Ni (and one case in Co) reported in the literature is shown in Table 4, demonstrating the excellent performance of our catalysts.

## Conclusions

This work presented a new bimetallic CoNi support for Pd nanocatalyst, fabricated by wet chemical reduction assisted with magnetic field and using $H_2PtCl_6$ as the nucleating agent. Pd NPs at two precursor concentrations ($K_2PdCl_4$) of 0.5 and 0.75 mM were produced and deposited on the as-prepared metallic supports at varying Co:Ni ratios (9:1, 7:3, 5:5, 3:7, 1:9). The key challenge during the synthesis of $Co_x$-$Ni_y$_Pd catalyst was, first of all, preparing these structures in such a way that the CoNi nanowires are covered with palladium nanoparticles. The second limitation was necessity to obtain a balance between highly crystalline metallic Ni(Co) and highly disorder $Co_{0.75}Ni_{0.25}$ phases in the structure of NiCo NWs. XRD, STEM, HRTEM, and XPS analyses confirmed the incorporation of palladium on CoNi bimetallic NWs and its appearance in metallic Pd and oxide $PdO_2$ forms. The catalytic activity tests

**Table 4 – Comparison of the mass activities of the as-prepared Co:Ni_Pd catalyst with other catalyst systems based on Pd, Ni or Co.**

| Catalyst | Electrolyte | Mass activity [mA/$mg_{Pd}$] | Reference |
|---|---|---|---|
| Pd modified Ni NW | 0.5 M KOH + 0.5 M Ethanol | 1480 | [67] |
| $Pd_2Ni_1$/C | 1.0 M NaOH + 1 M Ethanol | 2957 | [89] |
| NiCoPd/CNT | 1.0 M NaOH + 1 M Methanol | 862 | [73] |
| $Pd_{83}Ni_{17}$ HNS aerogel electrocatalyst | 1.0 M NaOH + 1 M Ethanol | 3630 | [90] |
| $Co_1$–$Ni_9$_Pd $_{(0.5mmol)}$ | 1 M NaOH + 0.5 M Ethanol | 3148 | This work |
| $Co_3$–$Ni_7$_Pd $_{(0.5mmol)}$ | 1 M NaOH + 0.5 M Ethanol | 5252 | This work |
| $Co_3$–$Ni_7$_Pd $_{(0.75mmol)}$ | 1 M NaOH + 0.5 M Ethanol | 8003 | This work |

showed that the obtained system can be successfully used as a catalyst in fuel cells powered by ethanol. The decoration of CoNi NWs by Pd NPs leads to a much higher availability of the palladium surface deposited on CoNi nanowires. As was shown, it has the effect of improving catalytic activity, because the connection between Pd and CoNi NWs plays a crucial role in the catalyst response. When Co:Ni ratio was equal to 1:9, palladium crystallized in metallic form, and the crystallites were large. The existence of these well crystalized Pd nanoparticles was responsible for excellent catalytic activity (2500 mA/$mg_{Pd}$ for 1.92% of Pd).

However, the best response was obtained for NWs, in which Co:Ni ratio was equal to 3:7 for both Pd loadings 0.5 and 0.75 mM. For this material, it was confirmed that the palladium crystallized mainly in the $PdO_2$ form at the oxidized surface and as metallic Pd atomic clusters on the metallic support. The coexistence of these two forms (Pd and $PdO_2$) and balance between metallic Ni(Co) and oxidized layer composed of $Co_3O_4$, NiO, and $Ni_2O_3$ allowed to achieve unexpectable high catalytic activity equal to 8003 mA/mgPd for only 0.86 wt% of Pd loading on the CoNi nanowire surface. Summarizing, the results obtained in the present work showed that by simultaneous consideration of the optimal chemical composition, crystallographic structure and well-defined shape of the novelty designed catalysts, the overall catalytic activity could be definitely improved. These three features represent a very important potential of newly designed catalysts described in this work. Thanks to combining of both composition and shape, the synthesis of a novel generation of efficient and more active catalyst toward ethanol oxidation reaction turned out to be possible. In addition, a novelty is also the replacement of the carbon support by bimetallic nanowires, what allow to avoid the detachment problems and corrosion of support. Both of selected metals (Ni and Co) have oxophilic nature and both of them take part in the catalytic reaction. Due to their oxophilic nature, it could spontaneously convert Ni and Co to their oxides. It is associated with the generation of active OH species, which oxidize the molecules adsorbed on the surfaces, facilitate CO removal, increase the tolerance to the poisoning of the noble metal by CO and finally enhance the catalytic activity. The innovativeness of the obtained system is also related to the lack of platinum in the proposed catalytic system, what is one of the biggest challenges when designing catalysts especially due to the economic terms. Moreover platinum is susceptible to poisoning by EOR by-products. As was shown in this work, it is possible to obtain efficient novelty platinum-free nanocatalysts with high catalytic activity in EOR. As a conclusion, this study clearly indicates that the developed Pd/CoNi catalytic system can be successfully used as an efficient electrocatalyst for ethanol oxidation in DEFCs (Direct Ethanol Fuel Cells) in an alkaline medium. In the future, the others metal nanoparticles will be tested with connection of CoNi nanowires.

## Declaration of competing interest

The authors declare that they have no known competing financial interests or personal relationships that could have appeared to influence the work reported in this paper.

## Acknowledgment

Tomasz Wasiak would like to thank the Silesian University of Technology for the financial support of this research [04/020/BKM21/1026, BKM-522/RCH-2/2021]. Dawid Janas would like to acknowledge the National Center for Research and Development, Poland [under the Leader program, grant agreement LIDER/0001/L-8/16/NCBR/2017]. Dariusz Łukowiec would also thank the Silesian University of Technology for the financial support of the research [10/100/BKM_21/0007, BKM-696/RMTL1/2021 and 10/010/SDU20/10-21-02]. Dariusz Łukowiec is a scholarship holder of the Visegrad International Scholarship Grant [ID: 52111121] for the period from September 2021 to June 2022.

## Appendix A. Supplementary data

Supplementary data related to this article can be found at https://doi.org/10.1016/j.ijhydene.2021.11.177.

## REFERENCES

[1] Marks-Bielska R, Bielski S, Pik K, Kurowska K. The importance of renewable energy sources in Poland's energy mix. Energies 2020;13. https://doi.org/10.3390/EN13184624. 4624 2020;13:4624.
[2] Qerimi D, Dimitrieska C, Vasilevska S, Rrecaj AA. Modeling of the solar thermal energy use in urban areas. Civ Eng J 2020;6:1349–67. https://doi.org/10.28991/CEJ-2020-03091553.

[3] Pirzada MJ, Memon SA, Das BN, Ali F, Gabol NA, Abro AW. Synthetic grey water treatment through FeCl3-activated carbon obtained from cotton stalks and river sand. Civ Eng J 2019;5:340–8. https://doi.org/10.28991/CEJ-2019-03091249.
[4] Priscilla SJ, Judi VA, Daniel R, Sivaji K. Emerging science journal effects of chromium doping on the electrical properties of ZnO nanoparticles, vol. 4; 2020. https://doi.org/10.28991/esj-2020-01212.
[5] Greeley J, Markovic NM. The road from animal electricity to green energy: combining experiment and theory in electrocatalysis. Energy Environ Sci 2012;5:9246–56. https://doi.org/10.1039/C2EE21754F.
[6] Ruiz-Camacho B, Medina-Ramírez A, Villicaña Aguilera M, Minchaca-Mojica JI. Pt supported on mesoporous material for methanol and ethanol oxidation in alkaline medium. Int J Hydrogen Energy 2019;44:12365–73. https://doi.org/10.1016/J.IJHYDENE.2019.01.180.
[7] Hu GZ, Nitze F, Jia X, Sharifi T, Barzegar HR, Gracia-Espino E, et al. Reduction free room temperature synthesis of a durable and efficient Pd/ordered mesoporous carbon composite electrocatalyst for alkaline direct alcohols fuel cell. RSC Adv 2013;4:676–82. https://doi.org/10.1039/C3RA42652A.
[8] Liu X, Xu G, Chen Y, Lu T, Tang Y, Xing W. A strategy for fabricating porous PdNi@Pt core-shell nanostructures and their enhanced activity and durability for the methanol electrooxidation. Sci Rep 2015;5:1–6. https://doi.org/10.1038/srep07619. 2015 51.
[9] Barragán VM, Heinzel A. Estimation of the membrane methanol diffusion coefficient from open circuit voltage measurements in a direct methanol fuel cell. J Power Sources 2002;104:66–72. https://doi.org/10.1016/S0378-7753(01)00896-5.
[10] Verma A, Basu S. Direct use of alcohols and sodium borohydride as fuel in an alkaline fuel cell. J Power Sources 2005;145:282–5. https://doi.org/10.1016/J.JPOWSOUR.2004.11.071.
[11] Bianchini C, Shen PK. Palladium-based electrocatalysts for alcohol oxidation in half cells and in direct alcohol fuel cells. Chem Rev 2009;109:4183–206. https://doi.org/10.1021/CR9000995.
[12] Antolini E. Catalysts for direct ethanol fuel cells. J Power Sources 2007;170:1–12. https://doi.org/10.1016/J.JPOWSOUR.2007.04.009.
[13] Xu C, Tian Z, Shen P, Jiang SP. Oxide (CeO2, NiO, Co3O4 and Mn3O4)-promoted Pd/C electrocatalysts for alcohol electrooxidation in alkaline media. Electrochim Acta 2008;53:2610–8. https://doi.org/10.1016/J.ELECTACTA.2007.10.036.
[14] Tan JL, De Jesus AM, Chua SL, Sanetuntikul J, Shanmugam S, Tongol BJV, et al. Preparation and characterization of palladium-nickel on graphene oxide support as anode catalyst for alkaline direct ethanol fuel cell. Appl Catal A Gen 2017;531:29–35. https://doi.org/10.1016/J.APCATA.2016.11.034.
[15] Ayoub JMS, Geraldes AN, Tusi MM, Spinacé EV, Neto AO. Preparation of PtSnSb/C by an alcohol reduction process for direct ethanol fuel cell (DEFC). Ionics 2011;17:559–64. https://doi.org/10.1007/S11581-011-0574-Y. 2011 176.
[16] Spinacé EV, Linardi M, Neto AO. Co-catalytic effect of nickel in the electro-oxidation of ethanol on binary Pt–Sn electrocatalysts. Electrochem Commun 2005;7:365–9. https://doi.org/10.1016/J.ELECOM.2005.02.006.
[17] Geissler K, Newson E, Vogel F, Truong T-B, Hottinger P, Wokaun A. Autothermal methanol reforming for hydrogen production in fuel cell applications. Phys Chem Chem Phys 2001;3:289–93. https://doi.org/10.1039/B004881J.
[18] Xu C, kang SP, Liu Y. Ethanol electrooxidation on Pt/C and Pd/C catalysts promoted with oxide. J Power Sources 2007;164:527–31. https://doi.org/10.1016/J.JPOWSOUR.2006.10.071.
[19] Farrell AE, Plevin RJ, Turner BT, Jones AD, O'Hare M, Kammen DM. Ethanol can contribute to energy and environmental goals. Science 2006;311(80):506–8. https://doi.org/10.1126/SCIENCE.1121416.
[20] Parrondo J, Santhanam R, Mijangos F, Rambabu B. Electrocatalytic performance of in 2 O 3-supported Pt/C nanoparticles for ethanol electro-oxidation in direct ethanol fuel cells. Int J Electrochem Sci 2010;5:1342–54.
[21] Song S, Tsiakaras P. Recent progress in direct ethanol proton exchange membrane fuel cells (DE-PEMFCs). Appl Catal B Environ 2006;63:187–93. https://doi.org/10.1016/J.APCATB.2005.09.018.
[22] Jiang L, Sun G, Wang S, Wang G, Xin Q, Zhou Z, et al. Electrode catalysts behavior during direct ethanol fuel cell life-time test. Electrochem Commun 2005;7:663–8. https://doi.org/10.1016/J.ELECOM.2005.04.021.
[23] Rousseau S, Coutanceau C, Lamy C, Léger JM. Direct ethanol fuel cell (DEFC): electrical performances and reaction products distribution under operating conditions with different platinum-based anodes. J Power Sources 2006;158:18–24. https://doi.org/10.1016/J.JPOWSOUR.2005.08.027.
[24] Shen SY, Zhao TS, Xu JB, Li YS. Synthesis of PdNi catalysts for the oxidation of ethanol in alkaline direct ethanol fuel cells. J Power Sources 2010;195:1001–6. https://doi.org/10.1016/J.JPOWSOUR.2009.08.079.
[25] Steele BCH, Heinzel A. Materials for fuel-cell technologies. Nature 2001;414:345–52. https://doi.org/10.1038/35104620. 2001 4146861.
[26] Drzymała E, Gruzeł G, Depciuch J, Pawlyta M, Donten M, Parlinska-Wojtan M. Ternary Pt/Re/SnO2/C catalyst for EOR: electrocatalytic activity and durability enhancement. Nano Res 2020;13:832–42. https://doi.org/10.1007/S12274-020-2704-1. 2020 133.
[27] Bensebaa Farid, Farah Abdiaziz A, Wang Dashan, Bock Christina, Du Xiaomei, Kung Judy, et al. Microwave synthesis of polymer-embedded Pt–Ru catalyst for direct methanol fuel cell. J Phys Chem B 2005;109:15339–44. https://doi.org/10.1021/JP0519870.
[28] Lamy C, Rousseau S, Belgsir EM, Coutanceau C, Léger JM. Recent progress in the direct ethanol fuel cell: development of new platinum–tin electrocatalysts. Electrochim Acta 2004;49:3901–8. https://doi.org/10.1016/J.ELECTACTA.2004.01.078.
[29] Antolini E. Palladium in fuel cell catalysis. Energy Environ Sci 2009;2:915–31. https://doi.org/10.1039/B820837A.
[30] Lee K, Kang SW, Lee S-U, Park K-H, Lee YW, Han SW. One-pot synthesis of monodisperse 5 nm Pd–Ni nanoalloys for electrocatalytic ethanol oxidation. ACS Appl Mater Interfaces 2012;4:4208–14. https://doi.org/10.1021/AM300923S.
[31] Silva JCM, Parreira LS, De Souza RFB, Calegaro ML, Spinacé EV, Neto AO, et al. PtSn/C alloyed and non-alloyed materials: differences in the ethanol electro-oxidation reaction pathways. Appl Catal B Environ 2011;110:141–7. https://doi.org/10.1016/J.APCATB.2011.08.036.
[32] Yang G, Namin LM, Aaron Deskins N, Teng X. Influence of *OH adsorbates on the potentiodynamics of the CO2 generation during the electro-oxidation of ethanol. J Catal 2017;353:335–48. https://doi.org/10.1016/J.JCAT.2017.07.033.
[33] Yu EH, Krewer U, Scott K. Principles and materials aspects of direct alkaline alcohol fuel cells. Energies 2010;3:1499–528. https://doi.org/10.3390/EN3081499. 2010;3:1499–528.
[34] Paik Y, Kim SS, Han OH. Spatial distribution of reaction products in direct ethanol fuel cell. Electrochem Commun 2009;11:302–4. https://doi.org/10.1016/J.ELECOM.2008.11.036.

[35] Mann J, Yao N, Bocarsly AB. Characterization and analysis of new catalysts for a direct ethanol fuel cell. Langmuir 2006;22:10432–6. https://doi.org/10.1021/LA061200C.
[36] Vigier F, Coutanceau C, Hahn F, Belgsir EM, Lamy C. On the mechanism of ethanol electro-oxidation on Pt and PtSn catalysts: electrochemical and in situ IR reflectance spectroscopy studies. J Electroanal Chem 2004;563:81–9. https://doi.org/10.1016/J.JELECHEM.2003.08.019.
[37] Yu EH, Scott K. Development of direct methanol alkaline fuel cells using anion exchange membranes. J Power Sources 2004;137:248–56. https://doi.org/10.1016/J.JPOWSOUR.2004.06.004.
[38] Burchardt T, Gouérec P, Sanchez-Cortezon E, Karichev Z, Miners JH. Alkaline fuel cells: contemporary advancement and limitations. Fuel 2002;81:2151–5. https://doi.org/10.1016/S0016-2361(02)00163-1.
[39] Jiang L, Hsu A, Chu D, Chen R. Size-dependent activity of palladium nanoparticles for oxygen electroreduction in alkaline solutions. J Electrochem Soc 2009;156:B643. https://doi.org/10.1149/1.3098478.
[40] Cui G, Song S, Shen PK, Kowal A, Bianchini C. First-principles considerations on catalytic activity of Pd toward ethanol oxidation. J Phys Chem C 2009;113:15639–42. https://doi.org/10.1021/JP900924S.
[41] Lim EJ, Kim Y, Choi SM, Lee S, Noh Y, Kim WB. Binary PdM catalysts (M = Ru, Sn, or Ir) over a reduced graphene oxide support for electro-oxidation of primary alcohols (methanol, ethanol, 1-propanol) under alkaline conditions. J Mater Chem A 2015;3:5491–500. https://doi.org/10.1039/C4TA06893A.
[42] Bambagioni V, Bianchini C, Marchionni A, Filippi J, Vizza F, Teddy J, et al. Pd and Pt–Ru anode electrocatalysts supported on multi-walled carbon nanotubes and their use in passive and active direct alcohol fuel cells with an anion-exchange membrane (alcohol = methanol, ethanol, glycerol). J Power Sources 2009;190:241–51. https://doi.org/10.1016/J.JPOWSOUR.2009.01.044.
[43] Antolini E, Gonzalez ER. Alkaline direct alcohol fuel cells. J Power Sources 2010;195:3431–50. https://doi.org/10.1016/J.JPOWSOUR.2009.11.145.
[44] Zhong J, Bin D, Yan B, Feng Y, Zhang K, Wang J, et al. Highly active and durable flowerlike Pd/Ni(OH)2 catalyst for the electrooxidation of ethanol in alkaline medium. RSC Adv 2016;6:72722–7. https://doi.org/10.1039/C6RA14321K.
[45] Lv X, Xu Z, Yan Z, Li X. Bimetallic nickel–iron-supported Pd electrocatalyst for ethanol electrooxidation in alkaline solution. Electrocatalysis 2011;2:82–8. https://doi.org/10.1007/S12678-011-0044-3. 2011 22.
[46] Xu CW, Wang H, Shen PK, Jiang SP. Highly ordered Pd nanowire arrays as effective electrocatalysts for ethanol oxidation in direct alcohol fuel cells. Adv Mater 2007;19:4256–9. https://doi.org/10.1002/ADMA.200602911.
[47] Yang H, Wang H, Li H, Ji S, Davids MW, Wang R. Effect of stabilizers on the synthesis of palladium–nickel nanoparticles supported on carbon for ethanol oxidation in alkaline medium. J Power Sources 2014;260:12–8. https://doi.org/10.1016/J.JPOWSOUR.2014.02.110.
[48] Gao Y, Wang G, Wu B, Deng C, Gao Y. Highly active carbon-supported PdNi catalyst for formic acid electrooxidation. J Appl Electrochem 2010;41:1–6. https://doi.org/10.1007/S10800-010-0201-Z. 2010 411.
[49] Bi Y, Lu G. Control growth of uniform platinum nanotubes and their catalytic properties for methanol electrooxidation. Electrochem Commun 2009;11:45–9. https://doi.org/10.1016/J.ELECOM.2008.10.023.
[50] Shang C, Hong W, Wang J, Wang E. Carbon supported trimetallic nickel–palladium–gold hollow nanoparticles with superior catalytic activity for methanol electrooxidation. J Power Sources 2015;285:12–5. https://doi.org/10.1016/J.JPOWSOUR.2015.03.092.
[51] Hoa LQ, Vestergaard MC, Yoshikawa H, Saito M, Tamiya E. Functionalized multi-walled carbon nanotubes as supporting matrix for enhanced ethanol oxidation on Pt-based catalysts. Electrochem Commun 2011;13:746–9. https://doi.org/10.1016/J.ELECOM.2011.03.041.
[52] Yin Z, Zheng H, Ma D, Bao X. Porous palladium nanoflowers that have enhanced methanol electro-oxidation activity. J Phys Chem C 2008;113:1001–5. https://doi.org/10.1021/JP807456J.
[53] Ghosh S, Raj CR. Facile in situ synthesis of multiwall carbon nanotube supported flowerlike Pt nanostructures: an efficient electrocatalyst for fuel cell application. J Phys Chem C 2010;114:10843–9. https://doi.org/10.1021/JP100551E.
[54] Zhang M, Yan Z, Xie J. Core/shell Ni@Pd nanoparticles supported on MWCNTs at improved electrocatalytic performance for alcohol oxidation in alkaline media. Electrochim Acta 2012;77:237–43. https://doi.org/10.1016/J.ELECTACTA.2012.05.098.
[55] Ma L, Chu D, Chen R. Comparison of ethanol electro-oxidation on Pt/C and Pd/C catalysts in alkaline media. Int J Hydrogen Energy 2012;37:11185–94. https://doi.org/10.1016/J.IJHYDENE.2012.04.132.
[56] Antolini E. Carbon supports for low-temperature fuel cell catalysts. Appl Catal B Environ 2009;88:1–24. https://doi.org/10.1016/J.APCATB.2008.09.030.
[57] Liu XN, Deng C, Gao Y, Wu B. Preparation of graphene and graphene supported Pd catalysts for formic acid electrooxidation. J Fuel Chem Technol 2014;42:476–80. https://doi.org/10.1016/S1872-5813(14)60023-2.
[58] Obradović MD, Stančić ZM, Lačnjevac U, Radmilović VV, Gavrilović-Wohlmuther A, Radmilović VR, et al. Electrochemical oxidation of ethanol on palladium-nickel nanocatalyst in alkaline media. Appl Catal B Environ 2016;189:110–8. https://doi.org/10.1016/J.APCATB.2016.02.039.
[59] Sheng J, Kang J, Hu Z, Yu Y, Fu X-Z, Sun R, et al. Octahedral Pd nanocages with porous shells converted from Co(OH)2 nanocages with nanosheet surfaces as robust electrocatalysts for ethanol oxidation. J Mater Chem A 2018;6:15789–96. https://doi.org/10.1039/C8TA04181D.
[60] Hosseini MG, Abdolmaleki M, Ashrafpoor S. Methanol electro-oxidation on a porous nanostructured Ni/Pd-Ni electrode in alkaline media. Chin J Catal 2013;34:1712–9. https://doi.org/10.1016/S1872-2067(12)60643-3.
[61] Qiu Z, Huang H, Du J, Feng T, Zhang W, Gan Y, et al. NbC nanowire-supported Pt nanoparticles as a high performance catalyst for methanol electrooxidation. J Phys Chem C 2013;117:13770–5. https://doi.org/10.1021/JP400592X.
[62] Cheng K, Jiang J, Kong S, Gao Y, Ye K, Wang G, et al. Pd nanoparticles support on rGO-C@TiC coaxial nanowires as a novel 3D electrode for NaBH4 electrooxidation. Int J Hydrogen Energy 2017;42:2943–51. https://doi.org/10.1016/J.IJHYDENE.2016.11.156.
[63] Koenigsmann C, Santulli AC, Gong K, Vukmirovic MB, Zhou W, Sutter E, et al. Enhanced electrocatalytic performance of processed, ultrathin, supported Pd–Pt core–shell nanowire catalysts for the oxygen reduction reaction. J Am Chem Soc 2011;133:9783–95. https://doi.org/10.1021/JA111130T.
[64] Mao J, Chen W, He D, Wan J, Pei J, Dong J, et al. Design of ultrathin Pt-Mo-Ni nanowire catalysts for ethanol electrooxidation. Sci Adv 2017;3:e1603068. https://doi.org/10.1126/SCIADV.1603068.
[65] Yan W, Wang D, Diaz LA, Botte GG. Nickel nanowires as effective catalysts for urea electro-oxidation. Electrochim

Acta 2014;134:266–71. https://doi.org/10.1016/J.ELECTACTA.2014.03.134.
[66] Tettamanti CS, Ramírez ML, Gutierrez FA, Bercoff PG, Rivas GA, Rodríguez MC. Nickel nanowires-based composite material applied to the highly enhanced non-enzymatic electro-oxidation of ethanol. Microchem J 2018;142:159–66. https://doi.org/10.1016/J.MICROC.2018.06.023.
[67] Kottayintavida R, Gopalan NK. Pd modified Ni nanowire as an efficient electro-catalyst for alcohol oxidation reaction. Int J Hydrogen Energy 2020;45:8396–404. https://doi.org/10.1016/J.IJHYDENE.2020.01.006.
[68] Hasan M, Newcomb SB, Rohan JF, Razeeb KM. Ni nanowire supported 3D flower-like Pd nanostructures as an efficient electrocatalyst for electrooxidation of ethanol in alkaline media. J Power Sources 2012;218:148–56. https://doi.org/10.1016/J.JPOWSOUR.2012.06.017.
[69] Wang C, Zheng L, Chang R, Du L, Zhu C, Geng D, et al. Palladium–cobalt nanowires decorated with jagged appearance for efficient methanol electro-oxidation. ACS Appl Mater Interfaces 2018;10:29965–71. https://doi.org/10.1021/ACSAMI.8B06851.
[70] Jiang Z, Wan W, Lin Z, Xie J, Chen JG. Understanding the role of M/Pt(111) (M = Fe, Co, Ni, Cu) bimetallic surfaces for selective hydrodeoxygenation of furfural. ACS Catal 2017;7:5758–65. https://doi.org/10.1021/ACSCATAL.7B01682.
[71] Miao B, Wu Z-P, Zhang M, Chen Y, Wang L. Role of Ni in bimetallic PdNi catalysts for ethanol oxidation reaction. J Phys Chem C 2018;122:22448–59. https://doi.org/10.1021/ACS.JPCC.8B05812.
[72] Zhang J, Xiang W, Liu Y, Hu M, Zhao K. Synthesis of high-aspect-ratio nickel nanowires by dropping method. Nanoscale Res Lett 2016;11:1–5. https://doi.org/10.1186/S11671-016-1330-Z. 2016 111.
[73] Zhang J-W, Zhang B, Zhang X. Enhanced catalytic activity of ternary NiCoPd nanocatalyst dispersed on carbon nanotubes toward methanol oxidation reaction in alkaline media. J Solid State Electrochem 2016;21:447–53. https://doi.org/10.1007/S10008-016-3331-3. 2016 212.
[74] Moulder JF, Stickle WF, Sobol PEBK. Handbook of X-ray photoelectron spectroscopy. MN, USA: Physical Electronics Inc.; 1995.
[75] Zhai X, Wang P, Wang K, Li J, Pang X, Wang X, et al. Facile synthesis of PtCo nanowires with enhanced electrocatalytic performance for ethanol oxidation reaction. Ionics 2020;26:3091–7. https://doi.org/10.1007/S11581-019-03419-1. 2020 266.
[76] Bonnelle JP, Grimblot J, D'huysser A. Influence de la polarisation des liaisons sur les spectres esca des oxydes de cobalt. J Electron Spectrosc Relat Phenom 1975;7:151–62. https://doi.org/10.1016/0368-2048(75)80047-8.
[77] Shafeev GA, Themlin J-M, Bellard L, Marine W, Cros A. Enhanced adherence of area-selective electroless metal plating on insulators. J Vac Sci Technol A Vac, Surf, Film 1998;14:319. https://doi.org/10.1116/1.579895.
[78] Jiang Y, Lu Y, Han D, Zhang Q, Niu L. Hollow Ag@Pd core–shell nanotubes as highly active catalysts for the electro-oxidation of formic acid. Nanotechnology 2012;23:105609. https://doi.org/10.1088/0957-4484/23/10/105609.
[79] Araujo RB, Martín-Yerga D, dos Santos EC, Cornell A, Pettersson LGM. Elucidating the role of Ni to enhance the methanol oxidation reaction on Pd electrocatalysts. Electrochim Acta 2020;360:136954. https://doi.org/10.1016/J.ELECTACTA.2020.136954.
[80] Liu Z, Zhang X, Hong L. Physical and electrochemical characterizations of nanostructured Pd/C and PdNi/C catalysts for methanol oxidation. Electrochem Commun 2009;11:925–8. https://doi.org/10.1016/J.ELECOM.2009.02.030.
[81] Qi Z, Geng H, Wang X, Zhao C, Ji H, Zhang C, et al. Novel nanocrystalline PdNi alloy catalyst for methanol and ethanol electro-oxidation in alkaline media. J Power Sources 2011;196:5823–8. https://doi.org/10.1016/J.JPOWSOUR.2011.02.083.
[82] Du C, Chen M, Wang W, Yin G. Nanoporous PdNi alloy nanowires as highly active catalysts for the electro-oxidation of formic acid. ACS Appl Mater Interfaces 2010;3:105–9. https://doi.org/10.1021/AM100803D.
[83] Bin D, Yang B, Ren F, Zhang K, Yang P, Du Y. Facile synthesis of PdNi nanowire networks supported on reduced graphene oxide with enhanced catalytic performance for formic acid oxidation. J Mater Chem A 2015;3:14001–6. https://doi.org/10.1039/C5TA02829A.
[84] Zamanzad Ghavidel MR, Monteverde Videla AHA, Specchia S, Easton EB. The relationship between the structure and ethanol oxidation activity of Pt-Cu/C alloy catalysts. Electrochim Acta 2017;230:58–72. https://doi.org/10.1016/J.ELECTACTA.2017.01.129.
[85] Lu Q, Huang J, Han C, Sun L, Yang X. Facile synthesis of composition-tunable PtRh nanosponges for methanol oxidation reaction. Electrochim Acta 2018;266:305–11. https://doi.org/10.1016/J.ELECTACTA.2018.02.021.
[86] Parlinska-Wojtan M, Drzymała E, Gruzeł G, Depciuch J, Donten M, Kowal A. Ternary Pt/Re/SnO2 nanoparticles for ethanol oxidation reaction: understanding the correlation between the synthesis route and the obtained material. Appl Catal A Gen 2019;570:319–28. https://doi.org/10.1016/J.APCATA.2018.11.030.
[87] Higuchi E, Takase T, Chiku M, Inoue H. Preparation of ternary Pt/Rh/SnO2 anode catalysts for use in direct ethanol fuel cells and their electrocatalytic activity for ethanol oxidation reaction. J Power Sources 2014;263:280–7. https://doi.org/10.1016/J.JPOWSOUR.2014.04.056.
[88] Crabb EM, Marshall R, Thompsett D. Carbon monoxide electro-oxidation properties of carbon-supported PtSn catalysts prepared using surface organometallic chemistry. J Electrochem Soc 2000;147:4440. https://doi.org/10.1149/1.1394083.
[89] Zhang Z, Xin L, Sun K, Li W. Pd–Ni electrocatalysts for efficient ethanol oxidation reaction in alkaline electrolyte. Int J Hydrogen Energy 2011;36:12686–97. https://doi.org/10.1016/J.IJHYDENE.2011.06.141.
[90] Cai B, Wen D, Liu W, Herrmann A-K, Benad A, Eychmüller A. Function-led design of aerogels: self-assembly of alloyed PdNi hollow nanospheres for efficient electrocatalysis. Angew Chem Int Ed 2015;54:13101–5. https://doi.org/10.1002/ANIE.201505307.